# Fatigue analysis of orthotropic steel-UHPFRC composite deck considering accelerated deterioration and self-healing of fractured UHPFRC in surface water condition

Chi Hieu Ma[a,*], Pengru Deng[c] and Takashi Matsumoto[b]

[a]*Graduate School of Engineering, Division of Engineering and Policy for Sustainable Environment*

*Hokkaido University, Kita-13, Nishi-8, Kita-ku, Sapporo 060-8628 Japan*

[b]*Faculty of Engineering, Division of Civil Engineering*

*Hokkaido University, Kita-13, Nishi-8, Kita-ku, Sapporo 060-8628 Japan*

[c]*School of Engineering, Central South University*

*No. 22, Shaoshan South Road, Tianxin District, Changsa City 410075 China*

*Email address:* chihieuma@gmail.com, pengrudeng@outlook.com and takashim@eng.hokudai.ac.jp; *Corresponding author.

**Abstract**

In this study, an orthotropic steel bridge deck overlaid with ultra-high-performance fiber-reinforced concrete (UHPFRC) is investigated using the finite element analysis. The composite bridge deck which is undergone moving-wheel load is examined under environmental surface water conditions. Two phases, i.e., Phases 1 and 2, are considered for the material model of the UHPFRC with stagnant water. In Phase 1, mechanical recoveries of the tensile strength and reloading stiffness are considered for the cracked UHPFRC caused by the autogenous self-healing behavior. In Phase 2, under the moving-wheel load, the crack bridging stress degradation in reinforced overlayer accelerates due to the closing–opening actions of surface cracks in water. In both phases, the deformation behaviors of the steel deck plate and UHPFRC overlayer are numerically examined. The results of the current numerical model agree with the experimental data in terms of the strain tendency, wherein the strain

range of the steel deck plate and UHPFRC overlayer decreases in Phase 1 and progressively increases in Phase 2. Therefore, it can be asserted that, under the surface water condition, scenarios considering two phases of the material model of cracked UHPFRC, have governed the strain behaviors of the tested composite bridge deck.

**Key words:** UHPFRC, OSD, fatigue, crack bridging stress degradation, self-healing behavior, FEA

## 1. Introduction

In recent years, ultra-high-performance fiber-reinforced concrete (UHPFRC) with excellent properties, such as high tensile and compressive strengths and high fatigue durabilities, has been used to cover the top surfaces of orthotropic steel bridge decks (OSDs), creating a reinforcing layer to improve structural fatigue performance. Following such modifications, the overall stiffness of OSDs has been observed to increase, leading to remarkable reductions in fatigue stress levels in the steel members of the OSDs. Thus, the fatigue durability of OSDs can be improved with the application of UHPFRC overlayers (Dieng et al., 2013; Makino et al., 2021, Deng et al., 2021, Ma et al., 2021a, Mi, 2020; Deng et al., 2022). It has been reported that, with such a thin thickness 25-mm of UHPFRC overlayer, the maximum magnitudes of displacement and stress level obtained in steel deck plate were notably reduced by over 37% and 88%, respectively (Makino et al., 2021).

However, for steel bridge decks covered by UHPFRC, stagnant water resulting from rainfall may adversely affect the structural performance of the reinforcing overlayer when subjected to repetitive traffic loading. Such stagnant water may pool over the UHPFRC, consequently subjecting the composite bridge deck to surface water conditions. Following this, the surface water may penetrate into microcracks on the top layer of the reinforced overlayer, further leading to severe fatigue deteriorations in the UHPFRC overlayer under moving-wheel loads. Matsui examined the effect of surface water on the structural performance of RC bridge decks (Matsui, 1987; Matsui, 1996). The results indicated that stagnant water on the top surface of RC bridge decks considerably degraded

their fatigue performance, and the fatigue life of the RC bridge decks reduced about 5% when the fatigue test was conducted under surface water condition (Matsui, 1996). Along similar lines, several experimental studies on the fatigue performance of concrete have been conducted in the presence of water, and the results have revealed that water adversely affects the fatigue durability of concrete materials (Waagaard, 1982; Solwik and Saouma, 2000; Matsushita, 1980; Maekawa and Fujiyama, 2013). Under the rapid deformation of concrete cracks, i.e., the closing–opening actions of cracks under fatigue loading, a high pore water pressure can be induced owing to the dispersion of condensed water inside cracks (Solwik and Saouma, 2000). This may further rapidly deteriorate concrete materials when capillary pores are subjected to water pressure; these pores are often located at the vicinity of the aggregate/matrix interface (Maekawa and Fujiyama, 2013). According to Matsushita (Matsushita, 1980; Matsushita and Tokumitsu, 1979), when the applied minimum stress is zero, the stress range ratio $S_r$ at 2,000,000 cycles for concrete with the presence of water is about 70% of that under dry conditions. Herein, $S_r = \Delta\sigma / \sigma_{ult} = (\sigma_{max} - \sigma_{min})/\sigma_{ult}$; where $\sigma_{max}$ and $\sigma_{min}$ are applied maximum and minimum stresses, $\sigma_{ult}$ is limit stress of concrete material.

Without considering fatigue action of applied load, under water exposure, the self-healing capability of high-performance fiber-reinforced cement composites, such as engineered cementitious composite (ECC) and UHPFRC, with regard to crack closure and mechanical recovery has been previously investigated (Okuizumi et al., 2021; Herbert and Li, 2012, 2013; Zhang and Zhang, 2017; Li and Li, 2011; Kan and Shi, 2012; Kim et al., 2019; Cuenca and Serna, 2021). Owing to the low ratio of water to cement used in the design of ECCs or UHPFRC, extensive amounts of unhydrated cement grains may exist in the material matrix. Consequently, continued hydration of unreacted cement may occur at the fractured region in the presence of water, leading to the closure of cracks in the specimens under testing. In a study conducted by Okuizumi et al. (2021), UHPFRC was found to exhibit a high self-healing ability under water conditions based on a high crack closure rate, which was observed from the bottom section of UHPFRC beams that cracked owing to flexural loads. After

only 1 day of water exposure, the closure rate of the UHPFRC fine cracks within a width of 0.014 mm in the specimens could reach over 77%. Herbert and Li (2012, 2013) examined the self-healing behavior of ECCs in the natural environment. Along with the closure of ECC cracks, mechanical recoveries of the tensile cracking strength and reloading stiffness in ECC specimens were observed after crack self-healing under water conditions. Moreover, under wet–dry cycles, the autogenous healing characteristics of high tensile ductility ECC materials were investigated by Kan and Shi (2012). The results revealed that the tensile strength and maximum tensile strain of the cracked specimens at the reloaded stage were higher than those of the reference specimens under dry conditions.

This paper proposes a numerical model based on the finite element method (FEM) to simulate an OSD overlaid by UHPFRC in the testing condition of surface water, and this deck is loaded by a moving rubber-tire wheel. Two phases of the material model considering the self-healing behavior and degradation in the fatigue life of cracked UHPFRC are introduced in this study. The proposed numerical model is validated using the experimental data reported by Makino et al., 2021. The structural responses from the considered phases, i.e., the deformation of steel members and the cracking behaviors of the reinforcing overlayer, are investigated in the analyses. The effect of self-healing behavior in UHPFRC cracks is also evaluated by a parametric study in the first phase.

## 2. Testing conditions and considered phases for the material model of cracked UHPFRC

To examine the effectiveness of the UHPFRC overlayer in improving the fatigue life of an OSD, fatigue tests on a full-scale OSD were conducted under wheel loading and environmental conditions in the previous study (Makino et al., 2021). Fig. 1 illustrates the geometry of the investigated composite deck. The dimensions in transverse and longitudinal directions of the OSD were 2720 and 3300 mm, respectively. The bridge deck comprised a 12 mm steel deck plate covered by a UHPFRC layer with a thickness of 25 mm, seven longitudinal ribs, three cross beams and two main girders.

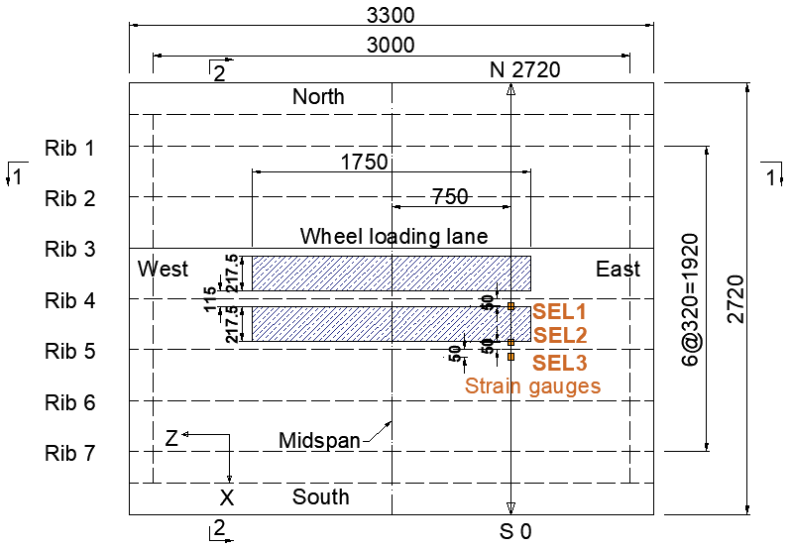


(a) Plan view

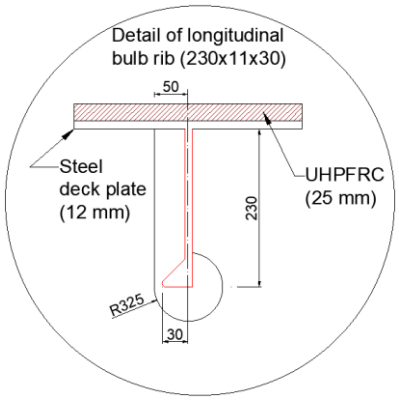


(b) Dimension of the longitudinal rib

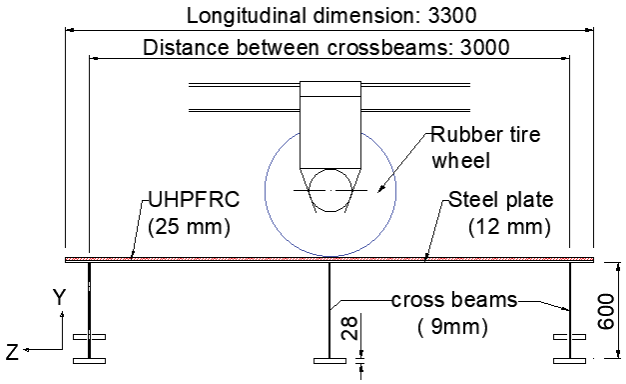


(c) Side view (cross section 1-1)

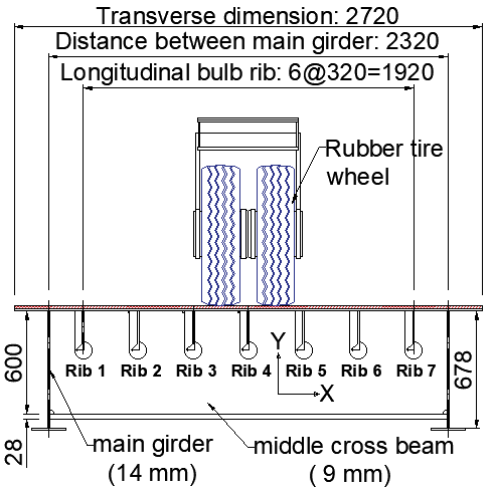


(d) Front view (cross section 2-2)

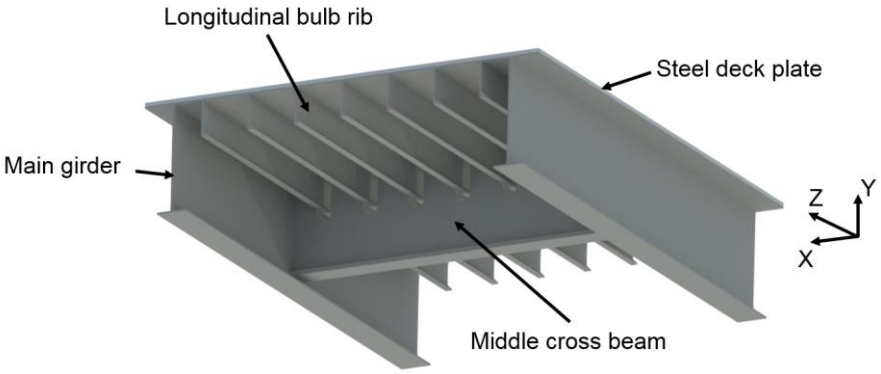


(e) 3D view of the current OSD (excluding East and West cross-beams)

Fig. 1 The OSD geometry (all dimensions are in mm)

The web thicknesses of the main girders and crossbeams were 14 and 9 mm, respectively. The dimensions of the longitudinal bulb ribs were 230 × 11 × 30 $mm^3$ (Fig. 1(b)).

The loading and environmental conditions adopted during the fatigue test for the composite bridge deck, and the fatigue test images of Stages 1 and 2 are depicted in Fig. 2. In the current study, fatigue analysis was conducted for Stage 2. After Stage 1, which included 1,100,000 cycles subjected to a moving wheel loaded with a rubber tire under dry conditions, the damaged composite deck with evident fine cracks on the top surface of the UHPFRC was subsequently tested for 60,000 cycles

under the surface water condition in 1 day. For one night before the execution of Stage 2 of the fatigue test, a thin layer of water was deposited on the overlayer top surface. In the current fatigue analysis, two phases were considered for the material model of cracked UHPFRC.

- Phase 1: self-healing of cracked UHPFRC in water for one night from the 1,100,000th to the 1,100,0001st loading cycle.
- Phase 2: higher degradation speed of cracked UHPFRC resulting from the combined action of fatigue wheel loading and surface water over 60,000 cycles.

The modeling of the behaviors for each phase of the cracked UHPFRC is detailed in Section 3.2.2.

| Testing conditions for two consecutive stages [2] | Stage | Load level (kN) | Number of cycles | Loading condition | Environmental condition |
|---|---|---|---|---|---|
| | Stage 1 | 100 | 1,100,000 | Rubber tire | Dry |
| | Stage 2 | 100 | 60,000 | Rubber tire | Surface water |

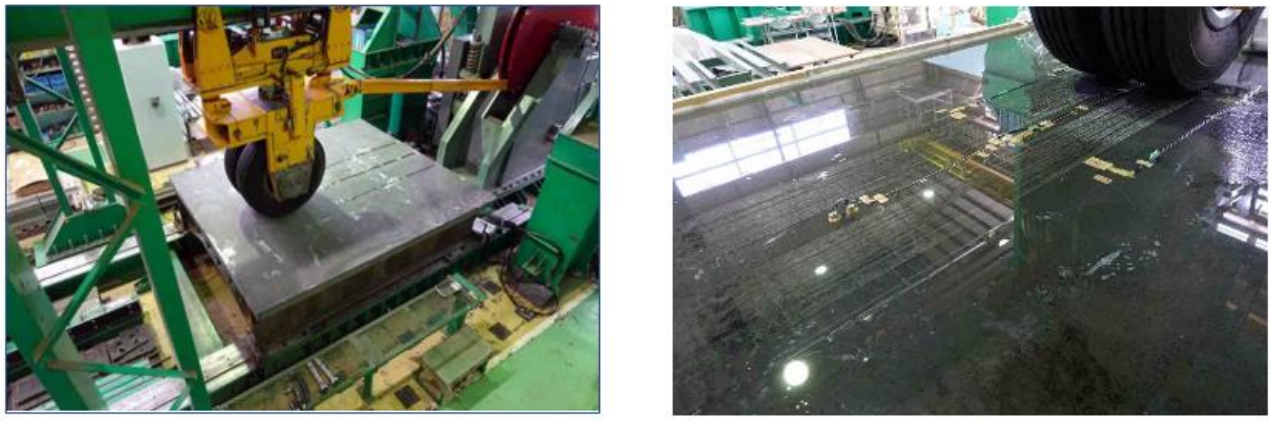

(a) Stage 1 (dry condition) (b) Stage 2 (surface water condition)

Fig. 2 Fatigue test of the OSD (Makino et al., 2021)

## 3. Method

### *3.1. Numerical model*

In this study, an OSD reinforced by UHPFRC overlayer undergone a moving load with a rubber tire under the surface water condition is simulated utilizing the FEM software MSC/Marc. Using Fortran programing language, a material user subroutine, which is applied to the Marc program to solve nonstandard problems, is coded to define the cracking behaviors of the UHPFRC. In the defined subroutine, the multi-fixed smeared crack model is applied to simulate crack initiation and development in the UHPFRC (Rots and Blaauwendraard, 1989). In this crack model, the original finite element mesh topology is maintained by transitioning from the initial isotropic stress-strain law

to an orthotropic relationship with the axes of orthotropy after the crack initiation. In other words, the smeared crack model assumes a cracked body as a continuum, while the discrete crack approach treats a crack as a discontinuous body with separated mesh elements. The initiation of UHPFRC cracks is predicted based on the direction and magnitude of the maximum principal stress generated in 3D UHPFRC eight-node elements. The first crack in the UHPFRC appears perpendicular to the maximum principal stress direction if the tensile stress level approaches the tensile cracking strength of the UHPFRC (i.e., value at point A in Fig. 4). Using a fixed crack model, the orientation of the initial crack is maintained in the UHPFRC overlayer during the calculation process. With the reorientation of the maximum principal stress when the wheel load moves, new cracks in the UHPFRC element initiate along planes orthogonal to the initial crack plane; this occurs when the cracking condition based on the maximum principal stress is satisfied.

Based on the procedure proposed by Rots and Blaauwendraard (1989), the overall stress–strain relationship in the UHPFRC element can be obtained using the following equation:

$$\sigma = D^{cocr}\varepsilon = \left[ D^{co} - D^{co}N(D^{cr} + N^T D^{co} N)^{-1} N^T D^{co} \right]\varepsilon , \quad (1)$$

where $\sigma$ and $\varepsilon$ denote the global stress and strain vectors, including the elastic and cracked components, respectively; $D^{co}$ and $D^{cr}$ denote the stiffness matrices of non-cracked and cracked components of the UHPFRC, respectively; $D^{cocr}$ denotes the overall stiffness matrix of the UHPFRC element; $N$ denotes the transformation matrix that defines crack orientation; and $N^T$ denotes the transpose of matrix $N$.

### *3.2. Material model*

#### *3.2.1. Steel*

The stress–strain relationship of the steel material, and the primary material properties of the steel members are presented in Fig. 3. Notably, a Poisson's ratio of 0.3 and Young's modulus of 200 GPa are considered in the current model. The von Mises criterion is used as the yield criterion of steel. In

the presence of the UHPFRC-strengthening layer, a significant decrease in stress levels was observed from the fatigue sensitive locations of the OSD, and no fatigue cracking was observed from the steel members. The fatigue of steel material was thus not prominent during the tested stages. In the current analysis, the fatigue life of steel members is estimated in Phase 1 (as mentioned in Section 2) to assess the beneficial effect of the self-healing behavior in UHPFRC cracks.

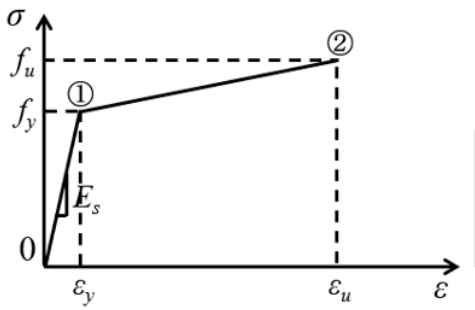


①: Yield strength, $(\varepsilon_y, f_y)$
②: Ultimate strength, $(\varepsilon_u, f_u)$

$$\sigma(\varepsilon)=\begin{cases} E_s\varepsilon & (\varepsilon \le \varepsilon_y) \\ f_y+\left(f_u-f_y\right)\left(\dfrac{\varepsilon-\varepsilon_y}{\varepsilon_u-\varepsilon_y}\right) & (\varepsilon_y<\varepsilon\le\varepsilon_u) \end{cases}$$

| | Parameter \ Steel members | | Cross beam | Longitudinal rib | Steel plate |
|---|---|---|---|---|---|
| Material properties of steel | Yield strength | $f_y$ (MPa) | 245 | 365 | 365 |
| | Tensile strength | $f_u$ (MPa) | 400 | 490 | 490 |
| | Ultimate tensile strain | $\varepsilon_u$ | 0.22 | 0.23 | 0.23 |

Fig. 3 Constitutive law and material properties of steel

*3.2.2. UHPFRC*

*3.2.2.1. Nonlinear constitutive law of UHPFRC*

A user subroutine in Marc program is coded to define the constitutive law of UHPFRC. According to JSCE Recommendations (2008), the nonlinear stress–strain relationships of UHPFRC are presented in Fig. 4. The constitutive law of UHPFRC under tension can be defined by a trilinear relation, i.e., (I) elastic, (II) strain-hardening, and (III) strain-softening domains. After the elastic domain, the tensile stress increases with the formation and propagation of microcracks in the second domain, i.e., the strain-hardening domain. Following this, localized macrocracks initiate and develop in the third domain after achieving the tensile strength.

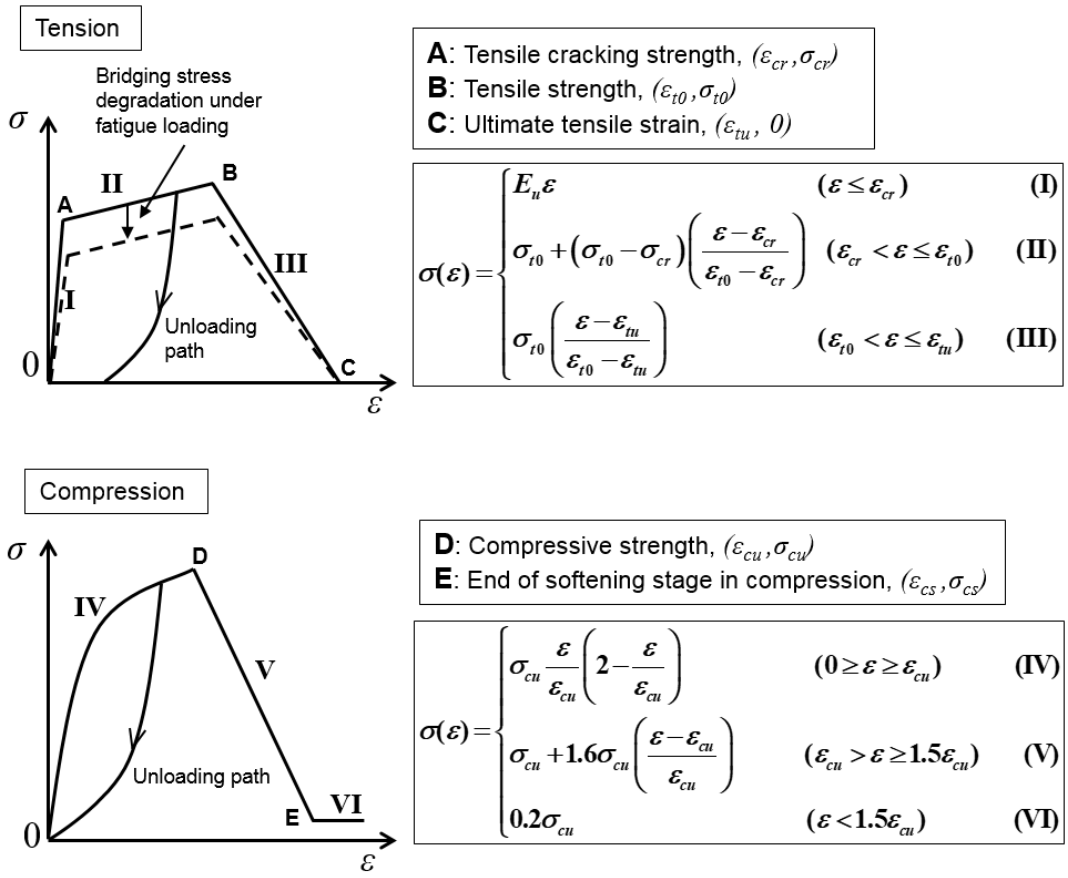


| | Parameter | Notation | Value (unit) | Point |
|---|---|---|---|---|
| Material properties of UHPFRC | Tensile cracking strength | $\varepsilon_{cr}$ | 0.00019 | A |
| | | $\sigma_{cr}$ | 6 (MPa) | |
| | Tensile strength | $\varepsilon_{t0}$ | 0.00175 | B |
| | | $\sigma_{t0}$ | 9 (MPa) | |
| | Ultimate tensile strain | $\varepsilon_{tu}$ | 0.01200 | C |
| | Compressive strength | $\varepsilon_{cu}$ | 0.0085 | D |
| | | $\sigma_{cu}$ | 133 (MPa) | |
| | Ending point of compressive softening stage | $\varepsilon_{cs}$ | 0.01275 | E |
| | | $\sigma_{cs}$ | 26.6 (MPa) | |

Fig. 4 Nonlinear stress–strain relationships and material properties of UHPFRC

The constitutive law of UHPFRC under compression can be defined by a parabolic relation in the (IV) fourth domain. When the compressive strength is reached, a linearly descending relation representing the softening law is used in the (V) fifth domain. Subsequently, the compressive stress presents a plateau at the end of the softening stage in the (VI) final domain.

For the elastic state, a Young's modulus ($E_u$) of 31.3 GPa and Poisson's ratio ($v$) of 0.22 were used in the analysis, following the in-site uniaxial compressive test of UHPFRC. The material properties referring to the UHPFRC material pamphlet provided by J-THIFCOM Construction Association (2020) are employed this study and summed in the embedded table in Fig. 4.

For shear stress transfer in the UHPFRC after the occurrence of tensile cracks, the progressive reduction in shear stiffness with an increase of tensile strain is considered in the current model (Fairbairn et al., 2006). A shear retention factor λ which is a function of the maximum tensile strain $\varepsilon_{tmax}$ is introduced in the analysis.

$$\lambda = \frac{1}{1 + 4447\varepsilon_{t\max}} \tag{2}$$

*3.2.2.2. Self-healing behavior of the cracked UHPFRC under surface water conditions*

Based on the studies conducted by Herbert and Li (2012, 2013), the mechanical recoveries of tensile strength and reloading stiffness of the UHPFRC surface cracks are considered in the current analysis, from the end stage of the dry condition (1,100,000th cycle) to the beginning stage of the surface water condition (1,100,001st cycle) in Phase 1 (Fig. 5).

The recovery ratios of the tensile strength, $\xi$, and reloading stiffness, $\kappa$, in the overlayer surface cracks are defined as follows:

$$\xi = \frac{\sigma_{1,100,001} - \sigma_{1,100,000}}{\sigma_1 - \sigma_{1,100,000}}, \tag{3}$$

$$\kappa = \frac{K_{1,100,001} - K_{1,100,000}}{K_1 - K_{1,100,000}}, \tag{4}$$

Where $\sigma_1$, $\sigma_{1,100,000,}$ and $\sigma_{1,100,001}$ denote the crack bridging stresses at the 1st, 1,100,000th, and 1,100,001st cycles, respectively; $K_1$, $K_{1,100,000}$ and $K_{1,100,001}$ denote the reloading stiffnesses at the 1st, 1,100,000th and 1,100,001st cycles, respectively.

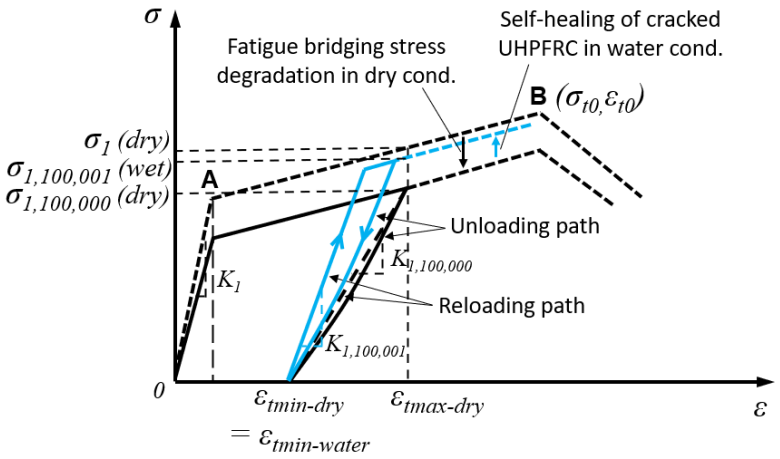


Fig. 5 Tensile stress–strain relation of the cracked UHPFRC under the surface water condition

The mechanical recoveries, especially for tensile strength, of the cracked UHPFRC under surface water condition are meaningful for the current fatigue test of Stage 2. By reducing the maximum tensile strain $\varepsilon_{tmax}$ of UHPFRC cracks after self-healing, the bridging stress degradation can thus be decelerated during fatigue loading, as referred to the Eqs. (5) - (6) in the next section.

Since the exposure time of the UHPFRC top layer in water is one night before the fatigue loading test, the tensile strength and reloading stiffness recovery ratios in this study are roughly chosen as 70%, $\kappa = \xi = 70\%$, following the observations from the research of Okuizumi et al. (2021).

*3.2.2.3. Fatigue degradation of UHPFRC crack bridging stress under the condition of surface water*

Under fatigue loading, the primary factor influencing crack development in various cement-based composites can be attributed to the gradual decrease in bridging stress between crack surfaces, which results from fatigue deterioration of tensioned fibers, i.e., fiber rupture or pullout (Li and Matsumoto, 1998; Matsumoto and Li, 1999; Zhang et al., 1999, 2000; Suthiwarapirak et al., 2004; Deng and Matsumoto, 2018; Jimi et al., 2021). For the UHPFRC, based on the study conducted by Jimi et al. (2021), the degradation law for the crack bridging stress under dry conditions is adopted in the current model for Stage 1 and is expressed as following equation:

213
$$\frac{\sigma_N}{\sigma_1} = 1 - (0.015 + 5\varepsilon_{t\max}) \log(N) \quad \text{for } 1 \le N \le 1{,}100{,}000 \tag{5}$$

214 where $\sigma_N/\sigma_1$ denotes the ratio of bridging stress degradation from $N$th to 1st cycles under dry condition.

215 According to researches of Matsushita (1980) for concrete material, when the applied minimum
216 stress is zero, the ratio of fatigue stress range at 2,000,000 cycles with the presence of water is about
217 70% of that under the dry condition. In the current study, by considering this reduced percentage from
218 the fatigue life of the concrete material to that of the UHPFRC, the corresponding degradation relation
219 of bridging stress for the overlayer cracks under the surface water condition is established and applied
220 in Phase 2.

221
$$\frac{\sigma_N}{\sigma_{1{,}100{,}001}} = 1 - (0.058 + 3.5\varepsilon_{t\max}) \log(N - 1{,}100{,}000) \quad \text{for } 1{,}100{,}001 \le N \le 1{,}160{,}000 \tag{6}$$

222 where $\sigma_N/\sigma_{1,100,001}$ denotes the ratio of bridging stress degradation from $N$th to 1,100,001st cycles
223 under the condition of surface water.

224 **4. Interfacial fatigue degradation between steel plate and UHPFRC**

225 In the current fatigue test, the UHPFRC overlayer was cast in place. Before applying the UHPFRC
226 layer, the shot blasting was used as a surface treatment technique to remove the contamination on the
227 surface of steel deck plate. After placing the epoxy bonding agent on steel deck plate with average
228 thickness of 1 mm, hard aggregates (i.e., synthetic ceramics) with a grain size of up to 2 mm were
229 distributed over the top surface of bonding agent to increase the surface roughness (Fig. 6(a)).
230 UHPFRC was then casted within the available time of epoxy bonding agent (i.e., within 5 minutes in
231 $20^{O}$C room temperature). According to the pull-off tensile test of composite specimens, the average
232 tensile bond strength of the current bonding technique was up to 2.91 MPa. For the epoxy resin
233 material at the interface between UHPFRC overlayer and steel plate, a linear elastic shear stress–

strain relationship is assumed in the current analysis (Fig. 6(a)). The shear elastic stiffness of the bond material, i.e., $E_{b1}$, is 2.66 GPa, is used following properties reported by Mitamura et al. (2011). In fatigue analysis of Stage 1, the interfacial bond stiffness degradation between steel plate and overlayer caused by repetitive moving-wheel load (see Fig. 6(a)) was considered by Ma et al. (2021). According to this study, by comparing the experimental observations (i.e., steel strain and hammer tapping test results) with the analysis results, the bond stiffness degradation speed was determined, as follows:

$$\frac{E_{bN}}{E_{b1}} = f(N) = 1 - 0.1707 \times \log(N) \quad \text{for } 1 \le N \le 700{,}000 \tag{7}$$

where $E_{bN}/E_{b1}$ denotes the ratio of the interfacial stiffness from $N$th to 1st cycles. The region being applied the bond stiffness degradation, S = 2×302×1875 mm$^2$, is shown in Fig. 6(c.I).

Subsequently, the delamination area at the interface was considered for the FEM model from the 700,000th cycle when the interfacial bond stiffness under wheel load region was zero (Ma et al., 2021). Fig. 6(b) shows the bonding layer at the UHPFRC/steel interface at the end of the experiment. The dark region under the wheel contact area, which comprised iron oxide particles obtained from shot-blasting process for the steel plate before applying the UHPFRC overlayer, could be observed after the fatigue test. This denoted the fatigue failure of bonding layer at wheel load region. In addition, based on acoustic inspections, i.e., a hammer test, in Stage 1 (see Fig. 6(c)), the abnormal noise range was detected at the 760,000th cycle, indicating the occurrence of interfacial delamination. Thereafter, the delamination area found by the hammer test gradually expanded in the local region above Rib 5. For the current model, the delamination area at the interface chosen at the initiating cycle of Stage 2 (1,100,001st) was equal to that at the ending cycle of Stage 1 (1,000,000th), as shown in Fig. 6(c.II). Throughout Stage 2, the average expansion speed of 4.67 mm/10,000 cycles along the transverse direction, which was applied to the interfacial debonded area, was selected identical to that of the

previous cycles in Stage 1 (from the 940,000th to the 1,100,000th cycles). The transverse dimension of the debonded area are then gradually increased from 840 to 868 mm (Fig. 6(c.III)).

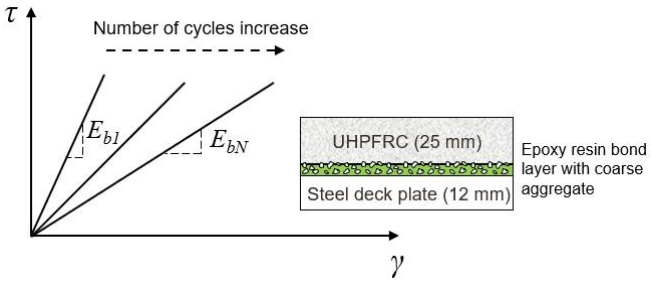


(a) Bond stiffness degradation model at steel/UHPFRC interface (Ma et al., 2021).

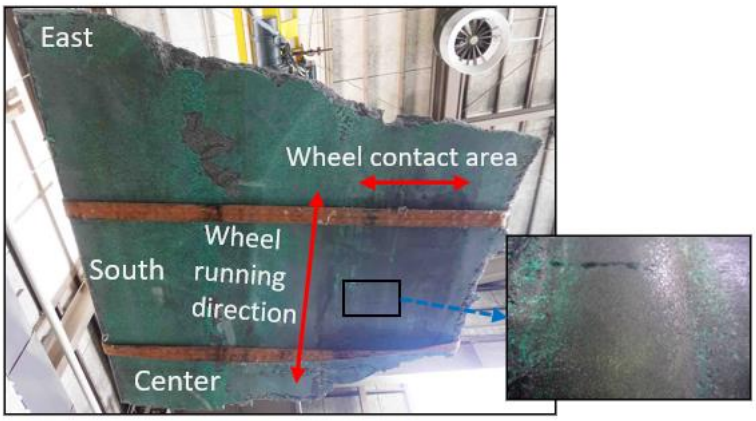


(b) Interfacial bond layer at the end of fatigue test (Makino et al., 2021).

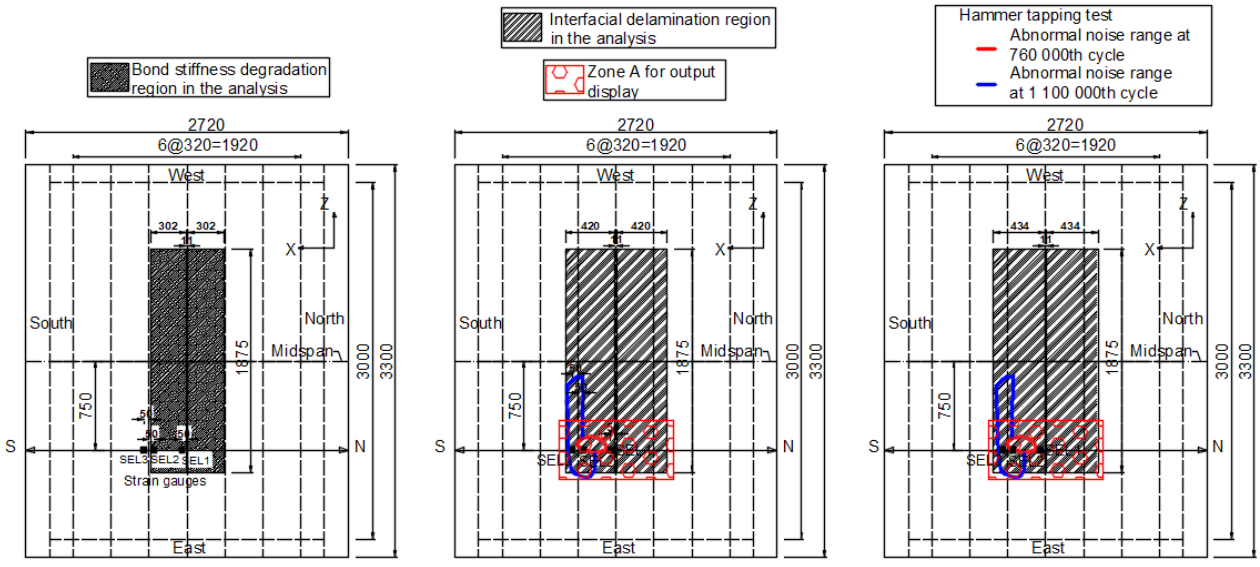


(c.I) Before 700,000 cycle (c.II) At 1,100,001st cycle (c.III) At 1,160,0010th cycle

(c) Interfacial degradation areas for fatigue analysis of Stage 2 (All dimensions are in mm)

Fig. 6 Interfacial degradation model in the fatigue analysis

## 5. Finite element modeling of the composite bridge deck

The boundary conditions and mesh pattern in the FEM model of the composite deck are shown in Fig. 7(a). Notably, a fine mesh with a minimum transverse size of 2.5 mm was employed for the overlayer and steel plate at regions above the three central longitudinal ribs. The UHPFRC-reinforced layer was vertically segregated into three layers in the current FEM model. In order to minimize computational cost, the 4-node thick shell elements are utilized instead of the 8-node solid elements to model the steel members such as cross beams, main girders, and the 4 outer bulb ribs (which are located far away from the critical region at wheel loading lane, as shown in Fig. 7(b)). It was found that, in comparison the model using only solid elements, the analysis time of the current model reduced about 40%, while the differences between numerical results at critical locations in steel deck plate of the two FE model are within 1%. The total number of elements used in the current FE model are 47,390.

Four edges under the main girders were supported with a 3000 mm longitudinal span. Two edges along the west side were restricted in all the three translational directions. The other edges from the east side were constrained against translation along the X and Y directions. The rubber tire wheel with a load of 100 kN was simulated using seven load locations. The size of each load location was $2 \times 217.5 \times 250$ mm$^2$, with a central gap of 115 mm, i.e., the distance between two tires. The 100-kN wheel-load was distributed over the whole area of load location, in which non-uniform distributions along the longitudinal and transverse directions of contact patch of rubber tire were based on the loading model presented by Ma et al. (2021), which has been reported to provide a better prediction of structural responses in steel deck plate than the standard uniformly-distributed load model. To simulate the interface between UHPFRC and steel plate in FEM model, the UHPFRC bottom layer and the steel-plate top surface are designated as deformable bodies of the contact analysis in MSC/Marc. The Touching contact option is used to model the interfacial delamination region (see Fig.6(c)), in which the material penetration is prevented. The remain interfacial region is simulated

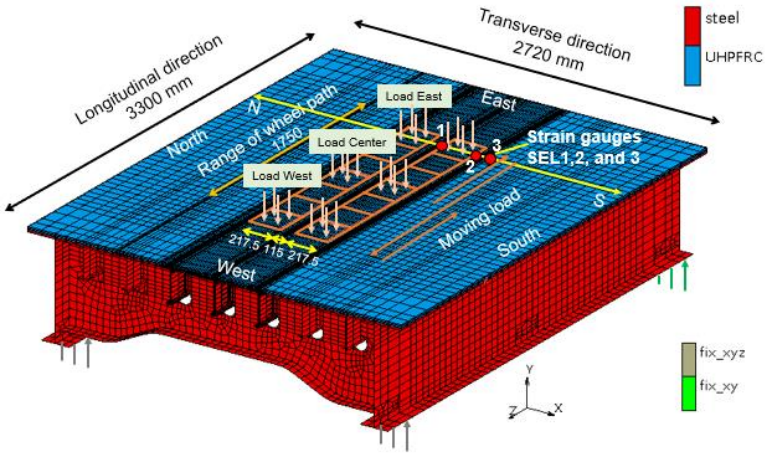


(a) Boundary conditions

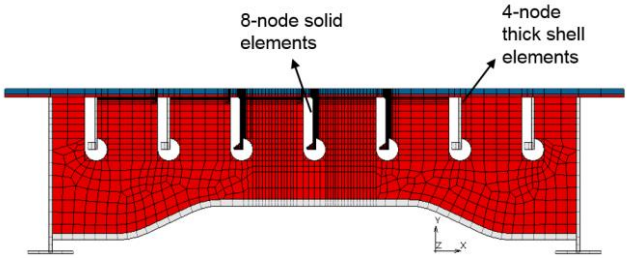


(b) Front view of FEM model

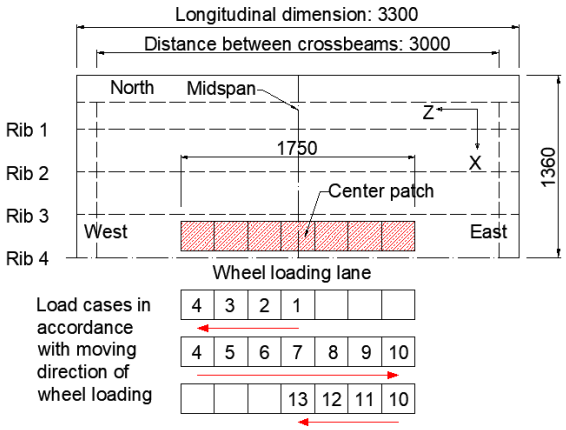


(c) Moving direction and load cases used in a single cycle

Fig. 7 FEM model of the composite deck (All dimensions are in mm)

by the Glue contact option, in which the interfacial contact stiffness between the deformable bodies is assigned to be the elastic modulus $E_{b1}$ of UHPFRC.

In the fatigue analysis, the moving direction of wheel loading under the specified load cases in a single cycle is presented in Fig. 7(c). The wheel load is initially applied to the central location until

302 the peak value (100 kN) is reached from load case 1. In load case 2, this location is unloaded with the
303 loading of the adjacent elements at the same increasing rate. Herein, each load case includes 30
304 loading steps with a total running time of 2190s. This procedure is continuously repeated along the
305 loading lane, reproducing the movement of the rubber tire wheel. During this process, the bridging
306 stress degradation equation (i.e., Eq. (6)) and unloading behaviors at each integration point of the
307 UHPFRC elements are modified and determined based on the maximum value of tensile strain, which
308 is recorded from the previous cycle of the fatigue analysis. The obtained bridging stress degradation
309 value at each node is then applied directly to the nonlinear constitutive law of UHPFRC after cracking
310 which is defined in the multi-fixed smeared crack model for each cycle. The current analysis of Stage
311 2 is performed for 60,000 cycles to reproduce the fatigue test under surface water condition.

312 **6. Results and discussions**

313 *6.1. Steel strains in the deck plate*

314 *6.1.1 Numerical steel strain distributions*

315 The distributions of the transverse strain under bottom surface of the steel deck plate for different
316 cycles are depicted in Fig. 8. The illustrated results are obtained from zone A (Fig. 6(c.II)) under load
317 case 10. Under load case 10, the positive bending at the tire contact region is produced by the wheel
318 load along with the overall downward movement of the steel deck plate. On the other hand, owing to
319 the stiffening effect of the longitudinal Ribs 3,4 and 5, the wheel load induces negative bending at
320 these local regions. At the 1,100,001st cycle (Phase 1), owing to an increase in the tensile strength of
321 the fine cracks in the UHPFRC overlayer after autogenous self-healing (Section 3.2.2), the overall
322 stiffness of the composite deck increases after one-night exposure to water. This leads to a decrease
323 in strain levels in the compressive zones at Ribs 3–5 and tensile zones at the wheel contact area of
324 the steel deck plate during this loading cycle. Further, the mechanical recoveries of the cracked
325 UHPFRC in Phase 1 can be interpreted based on the opening–closing actions of a single crack (Fig.

9) on the top layer of the overlayer before and after self-healing. It is noted that the UHPFRC tensile cracks at East patch above Ribs 3, 4 and 5 are under the process from opening to closing when the wheel load moves from East to West load patches; and vice versa. In the presence of the healed part inside the UHPFRC crack, the stress transfer between pulled-out or ruptured fibers is restored, causing an increase in the bridging stress between the crack surfaces. Thus, the reloaded maximum strain or crack opening displacement decreases after the self-healing of UHPFRC cracks (Fig. 9(d)). The autogenous healing process of the UHPFRC cracks is assumed to terminate at the beginning of the 1,100,001st cycle (Fig. 9(c)), and the healed parts undergo cracking and degradation under repetitive wheel loading without further self-healing throughout Stage 2. Therefore, the unloading

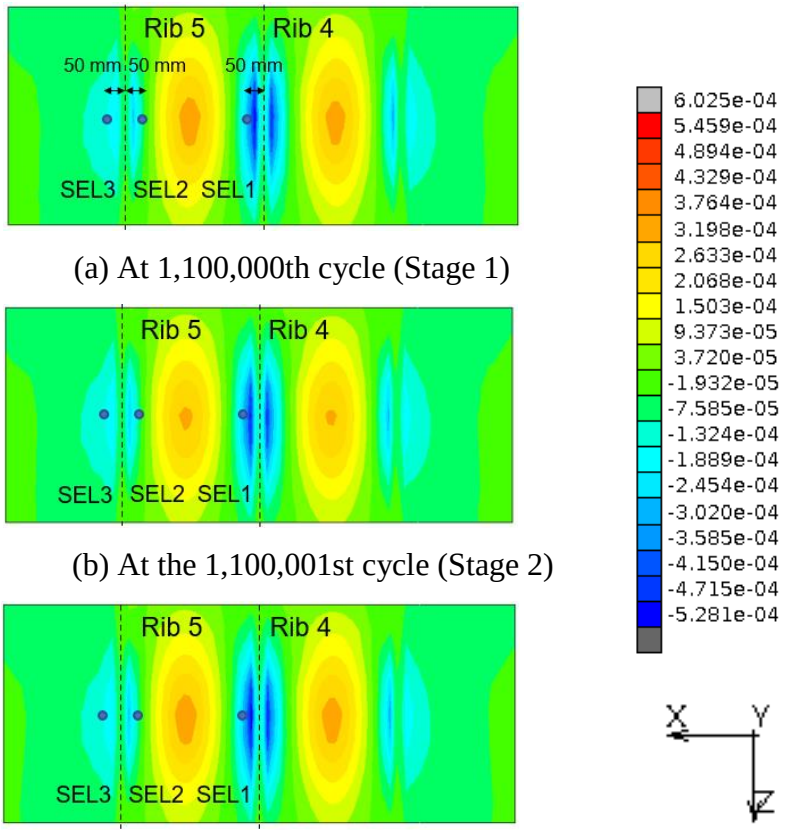


(a) At 1,100,000th cycle (Stage 1)

(b) At the 1,100,001st cycle (Stage 2)

(c) At the 1,160,000th cycle (Stage 2)

Fig. 8 Distributions of the steel transverse strain under bottom surface of the deck plate for different cycles in load case 10 (displayed at zone A).

minimum strain under the water condition ($\varepsilon_{tmin\text{-}water}$) is maintained equal to that under the dry condition ($\varepsilon_{tmin\text{-}dry}$) (Fig. 9(e)).

In contrast to the first cycle of Stage 2, the increase in transverse strain magnitudes can be observed at the 1,160,000th cycle (see Fig. 8(c)), and this is owing to fatigue bridging stress degradation of cracked UHPFRC under moving-wheel loading in Phase 2. After the formation of a tensile crack, owing to the continuous reduction in tensile strength resulting from the degradation in the bridging stress between crack surfaces, a stress concentration can be induced in the region of the crack tip. Thereafter, the fatigue crack propagates in the overlayer with a newly formed crack length at the crack tip. Consequently, the deformation of the bridge deck is increased, leading to strain redistribution in the UHPFRC and steel plate. Moreover, stiffness reduction of the bridge deck is as

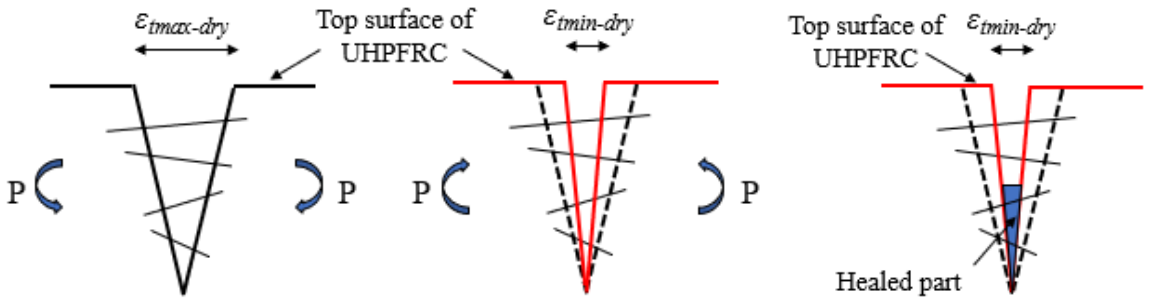


(a) Loading under dry condition (b) Unloading under dry condition (c) Healed part formed inside crack

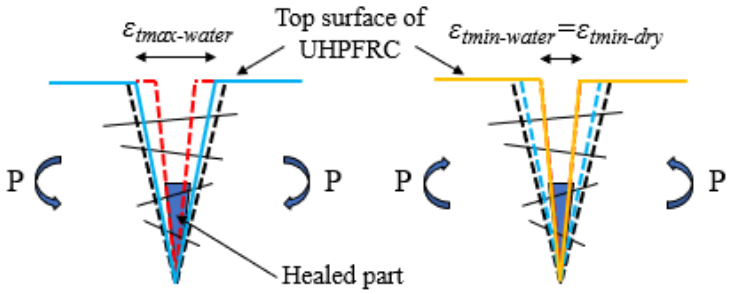


(d) Reloading under water condition (e) Unloading under water condition

Fig. 9 Opening–closing behaviors of a UHPFRC crack before (a and b) and after (d and e) self-healing.

well due to the expansion of the debonded area at steel/UHPFRC interface, which leads to a progressive loss in the capability of shear force transfer between the overlayer and steel plate. The degradation in crack bridging stress of UHPFRC, which are dependent on the maximum level of the tensile strain, is thus accelerated, along with the interfacial–delamination development. As a result, those kinds of fatigue degradations with their mutual interaction can considerably deteriorate the structural performance of the tested bridge deck.

*6.1.2 Numerical and experimental steel strain evolutions*

In Fig. 10, the transverse strain range evolutions in load case 10 at the locations of the SEL strain gauges (Fig. 1(a)) under steel-plate bottom are plotted in comparison with the experimental data, with the chosen recovery ratios for tensile strength and reloading stiffness of 70%. As reported by Ma et al. (2021), in Stage 1, owing to continuous deterioration of the interfacial bond stiffness before the 700,000th cycle, the strain range of the steel deck plate gradually decreases with an increase of the number of cycles. Subsequently, a delamination area formed at the UHPFRC/steel interface and expands along the transverse direction, leading to considerable variations in the transverse strain range levels of the steel deck plate from 700,000th to 1,100,000th cycles. From Fig. 10, it is apparent that the experimental strain range magnitudes at the SEL strain gauges from the end of Stage 1 (1,100,000th cycle) to the beginning of Stage 2 (1,100,001st cycle) have decreased after one-night exposure in surface water condition. Possible cause of this behavior is the self-healing of surface cracks in the overlayer, as introduced above. To assess the effect of this mechanism on the structural responses of the composite deck, a parametric study is conducted and presented in the following section.

*6.1.2.1 Effect of self-healing behaviors on strain responses in Phase 1*

Based on the current analysis under surface water condition in Phase 1, Fig. 11 shows the relationships between the recovery ratios of tensile strength and reloading stiffness caused by self-

384 healing, along with the results of the transverse strain range considering the reduction rates from the
385 1,100,001st cycle at strain gauge SEL1, i.e., steel plate's critical location. When the recovery ratios
386 after the self-healing of UHPFRC cracks increase, the transverse strain range levels at SEL1 decrease,
387 along with an increase in the reduction rates of the strain range. In the current model, with recovery
388 ratios of 100% for the UHPFRC surface cracks, the reduction in the transverse strain range at SEL1
389 can reach 7.32% (reduced from -267.7μ to -248.1μ). Based on the Japan Society of Steel Construction
390 (JSSC) code (1993), the prediction analysis of the fatigue life at the critical point of SEL1 is
391 conducted using the obtained transverse strain ranges. The fatigue life (in years) ($N$) is calculated as
392 follows:

393 $$N = \frac{n \times 100}{n_{ti-100}}$$

394 where $n = \frac{(FAT)^m \times (2 \times 10^6)}{\Delta\sigma_{eq}^m}$ is the number of cycles causing fatigue cracks; here, $FAT$ = 80 MPa

395 and $m$ = 3 for E-class welding design. $\Delta\sigma_{eq} = \sqrt[3]{\frac{\Sigma \Delta\sigma_i^3 \times n_i}{\Sigma n_i}}$ denotes the equivalent stress range, where

396 $\Delta\sigma_i$ denotes the stress range obtained in cycle $n_i$.

397 Further, $n_{ti-100} = ADTT_{SLi} \times \gamma_n \times 365 \times Y$ is the number of cycles corresponding to a design lifetime

398 of 100 years; here, $ADTT_{SLi}$ = 2880 (vehicles/day/lane) denotes the traffic volume, $\gamma_n = 0.03$ denotes

399 the frequency coefficient, and $Y$ = 100 (years) denotes the design service life of the composite bridge

400 deck. $N$ denotes the fatigue life in years.

401 The fatigue life prediction results at point SEL1 for different recovery ratios of tensile strength and

402 reloading stiffness are summarized in Table 1. The fatigue life of the OSD can be increased to a

403 maximum of 7.87% (from 258.9 to 279.3 years) when the self-healing recovery ratio of UHPFRC

404 cracks reaches 100%.

405

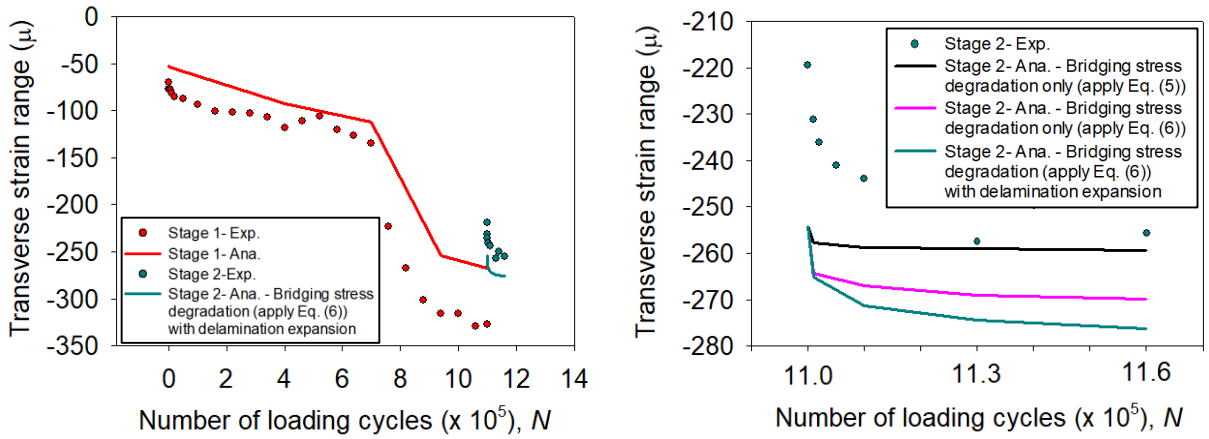


406

407 (a) SEL1

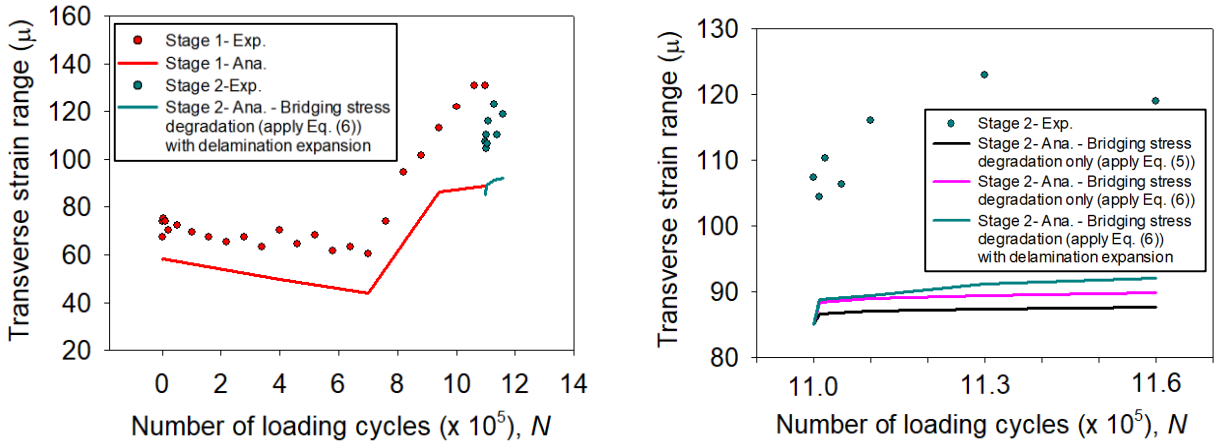


408

409 (b) SEL2

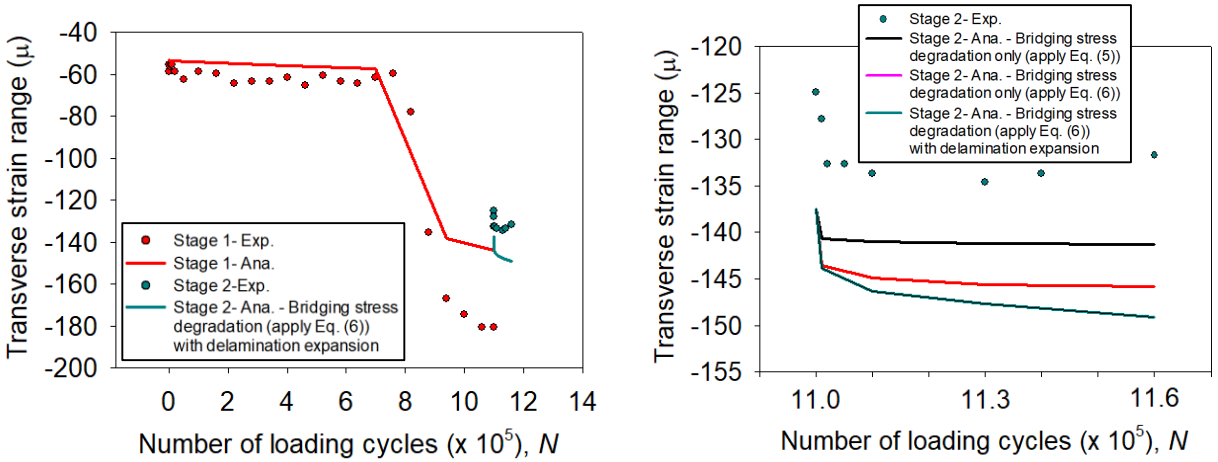


410

411 (c) SEL3

412 Fig. 10 Transverse strain range vs. the number of cycles at SEL strain gauges

413 In this self-healing phase, in the experiment with stagnant water, no material segregated on the top
414 surface of the UHPFRC. Such segregation can be identified based on a cloudy exudate of the
415 UHPFRC cracks. Fine cracks (hairline cracks) are observed on the overlayer surface at the beginning
416 of Stage 2 (see Fig. 16(b)). Therefore, the percentage of crack closure resulting from the self-healing
417 behavior is expected to be a high value after one-night exposure under the surface water condition,

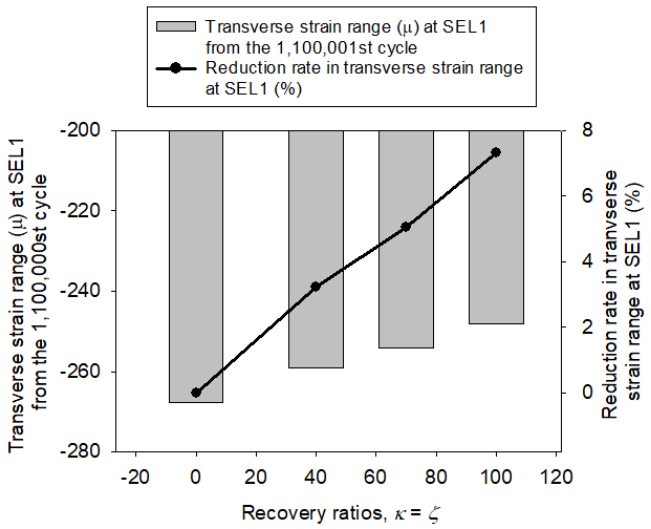


418

419 Fig. 11 Effect of the self-healing recovery ratio on the transverse strain range at SEL1

420

421 **Table 1**. Fatigue life prediction at a critical location of the steel deck plate

| Recovery ratio (%) $\kappa = \xi$ | Equivalent stress range (MPa) $\Delta\sigma_{eq}$ | Fatigue life (year) $N$ | Increasing rate in fatigue life (%) |
|---|---|---|---|
| 0 | 50.06 | 258.9 | 0 |
| 40 | 49.51 | 267.5 | 3.32 |
| 70 | 49.15 | 273.5 | 5.64 |
| 100 | 48.81 | 279.3 | 7.87 |

422

i.e., more than 70% based on the report for UHPFRC beams by Okuizumi et al. (2021). Following this, the recovery ratios of the tensile strength and reloading stiffness are set at values equal to the crack closure percentage and applied to the analysis.

*6.1.2.2 Effect of bridging stress degradation speed in Phase 2*

In fatigue analysis for Phase 2, the increased speed of crack bridging stress degradation of UHPFRC is considered as shown in Eq. (6). This results in a sharp increase in steel strain levels in the initial 5,000 cycles of Phase 2, as shown in Fig. 10. It is evident that the obtained results agree with the experimental data. In Figs. 10(a) and 10(c), the significant increase in the early cycles cannot be reproduced by the model using Eq. (5). Hence, it can be inferred that the increase in the bridging stress degradation speed may have occurred in the cracked UHPFRC under the moving-wheel load

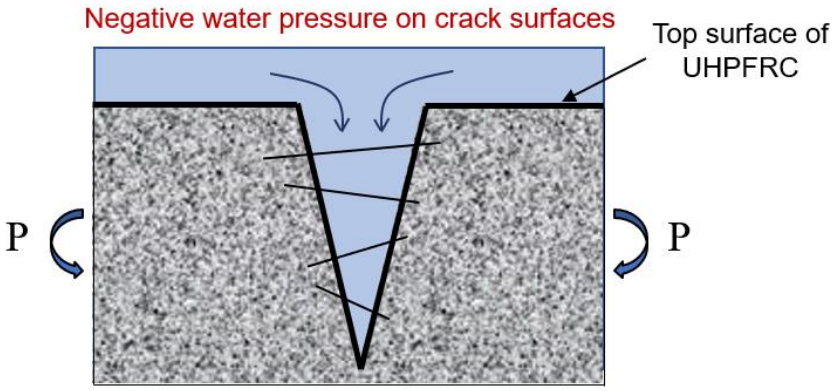


(a) Crack opening in water

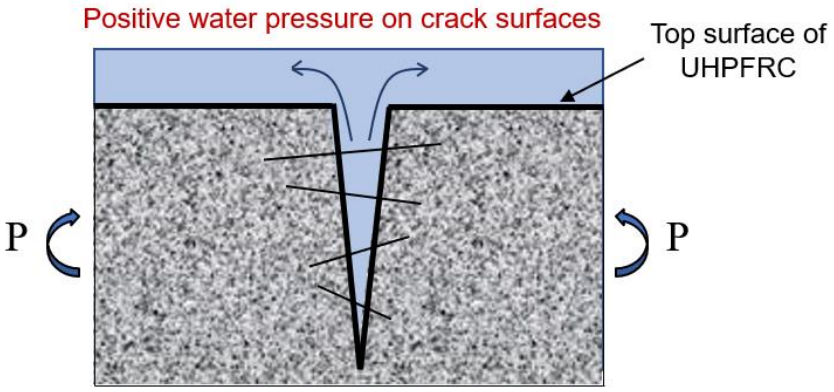


(b) Crack closure in water

Fig. 12 Water pressure generated inside a UHPFRC crack under cyclic loading

438 and surface water condition. This mechanism can be explained based on the generated water pressure
439 inside the cracks under repetitive cyclic loading (Fig. 12). Under cyclic loading, the water pressure
440 acting on the crack surfaces becomes negative with the opening of the UHPFRC crack. By contrast,
441 a positive water pressure can be obtained during the closure of the UHPFRC crack in the presence of
442 water. Hence, under the repetitive moving-wheel load, additional forces resulting from stagnant water
443 could accelerate fatigue fiber deterioration (i.e., fiber pullout) in the fractured zone, which may result
444 in an increase in the bridging stress degradation speed of UHPFRC cracks considered for Phase 2 of
445 the material model of the UHPFRC.

446 From Fig. 10, it is obvious that the contribution of bridging stress degradation to the increase in
447 the strain range is more dominant during the early stages of the fatigue analysis under the surface
448 water condition based on a comparison between numerical models with and without interfacial
449 delamination expansion. The reason for this is that the expansion of the debonded zone is quite
450 minimal at the beginning cycles of Phase 2. With an increase in the number of cycles, the strain ranges
451 of the steel plate increase, as the UHPFRC–steel composite undergoes continuous degradation when
452 the delamination area is expanded along the transverse direction.

453 Overall, the qualitative agreements in strain range tendencies could be obtained from the numerical
454 and experimental results of steel plate in the current study. Here, the proposed mechanisms for
455 UHPFRC material model under surface water condition (i.e., the self-healing in Phase 1 and the
456 accelerated fatigue degradation in Phase 2) are reasonable for reproducing the strain behaviors of the
457 tested composite deck. The parametric analyses conducted in each phase have clarified the effect of
458 each mechanism to the structural responses of steel bridge deck, as discussed above. However, from
459 the quantitative perspective, there are still discrepancies between the analysis and the experiment.
460 Following the research of Dai et al. (2005), it was shown that, along with the interfacial bond stiffness
461 degradation, the residual bond slip at zero-bond stress level also increased when the number of cycles
462 increased. Moreover, with a decrease in the tire-overlay friction coefficient owing to the presence of

water, the frictional force between the rubber tire and UHPFRC decreased. This may lead to additional transverse deformation at the edges of tire treads at tire contact region. Thus, in the experiment, the rubber tire contact region as well as the contact normal stresses in the surface water condition may be different from that under the dry condition. The residual bond slip at the UHPFRC/steel interface is thus affected by the contact condition of the rubber tire, i.e., in this case, the residual bond slip in the experiment may be increased. Owing to insufficient data on the current bonding technique at UHPFRC/steel interface, the residual bond strain between overlayer and steel plate under fatigue wheel loading is neglected in the current numerical model (Fig. 6(a)). This may lead to the underestimation of the unloading and reloading strain levels for the steel plate. Although experimental tendencies based on the strain range results can be relatively reproduced by the current model, the reproductions of unloading and reloading strain levels resulting from the residual bond slip at the interface, as well as the tire contact conditions in the presence of water can be considered in future studies on the composite bridge decks under moving-wheel loads.

### *6.2. Numerical strain of the UHPFRC overlayer*

#### *6.2.1 Numerical strain distributions*

The maximum strain distributions for the cracked elements during Stages 1 and 2 at zone A (presented in Fig. 6(c)) are shown in Fig. 13 for the bottom and top layers of the reinforced overlayer, respectively. The blue-to-red color band represents the cracked regions on the overlayer surface. For the OSD, an overall downward movement of the steel deck plate is achieved under wheel loading, which induces positive bending at the tire contact region. However, owing to the stiffening effect of the longitudinal rib, negative bending at these local regions is produced via wheel loading. Therefore, cracks emerge on the top surface of the overlayer and propagate at local zones above Ribs 3, 4, and 5; whereas tensile cracks at the bottom layer of the UHPFRC overlayer are created at the rubber-tire contact regions. At the beginning cycle of Stage 2, owing to an increase in the tensile strength caused

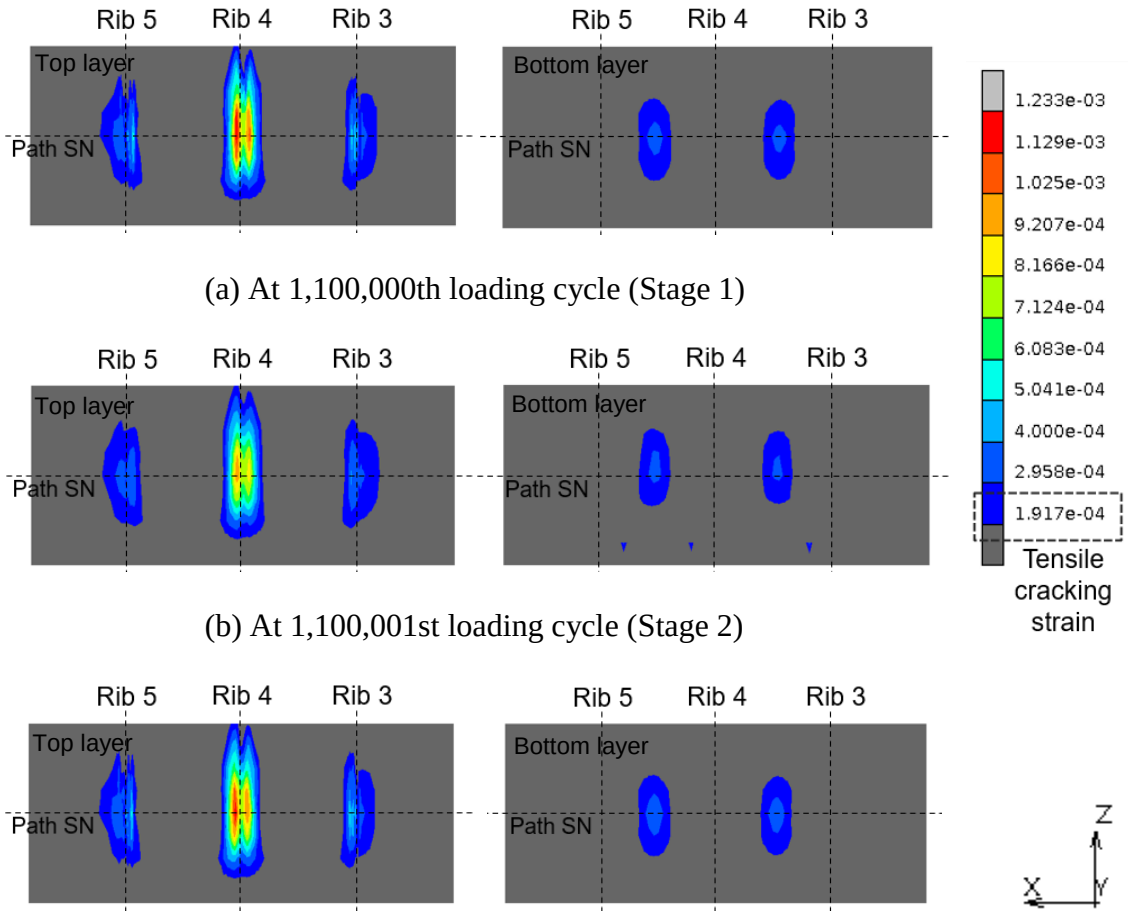


(a) At 1,100,000th loading cycle (Stage 1)

(b) At 1,100,001st loading cycle (Stage 2)

(c) At 1,160,000th loading cycle (Stage 2)

Fig. 13 Distributions of maximum principal strain for cracked areas on top and bottom layers of UHPFRC overlay (displayed at zone A)

by the self-healing of the cracks on the top layer of the UHPFRC, the maximum tensile strain levels from the top and bottom layers of the UHPFRC overlayer, as shown in Fig. 13(b), decrease compared to those under the dry condition (Fig. 13(a)). This is accompanied by a narrower crack region from the bottom layer of the overlayer. On the contrary, the maximum tensile strain level of UHPFRC increases at the end of this stage owing to a significant increase in the bridging stress degradation speed of the healed UHPFRC in stagnant water, as shown in Fig. 13(c).

The maximum principal strain directions obtained from the crack elements in the UHPFRC overlayer under load case 10 of the 1,160,000th cycle are depicted in Fig. 14. It is obvious that the maximum principal strain directions obtained from the crack elements on the UHPFRC top surface

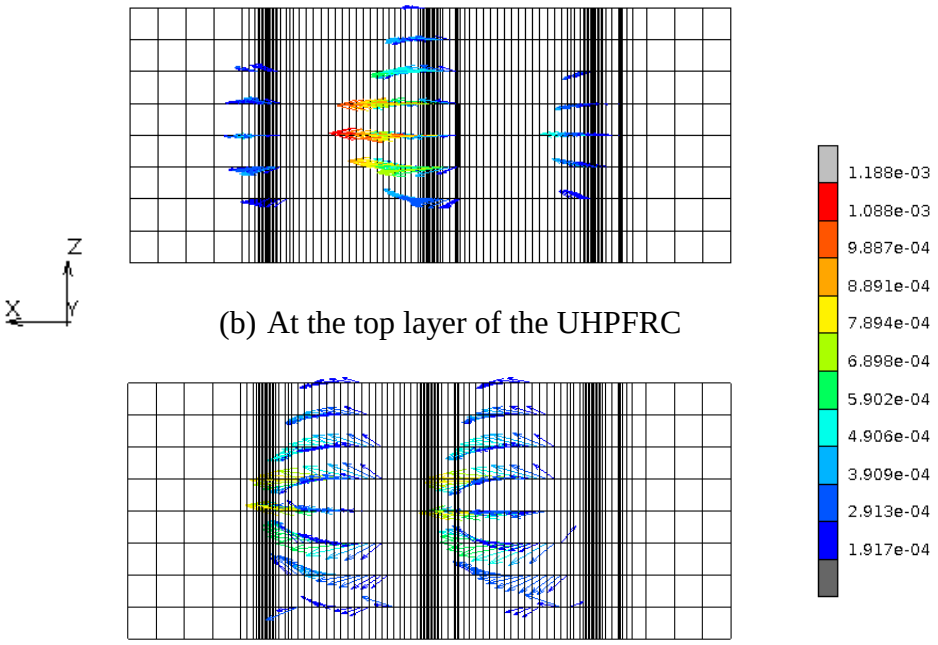


(b) At the top layer of the UHPFRC

(b) At the bottom layer of the UHPFRC

Fig. 14 Maximum principal strain directions of UHPFRC cracks at 1,160,000th loading cycle

are transverse (Fig. 14(a)). This implies that the UHPFRC cracks initiate and propagate along the longitudinal direction along Ribs 3, 4, and 5. On the other hand, diagonal cracks are observed from the bottom layer of the UHPFRC overlayer, and distributed around the east-load-patch centerline (see Fig. 14(b)). In the current model, it is found that that the second or third cracks in the UHPFRC elements are not formed after the initiation of the first cracks (Fig. 13). This is because the obtained stress levels along the longitudinal and vertical directions from the crack elements in the UHPFRC overlayer are much smaller than those along the transverse direction, which can be attributed to the stiffening effect of the longitudinal ribs and relative thin thickness of the applied UHPFRC overlayer.

*6.2.2 Numerical strain evolution at the critical location of UHPFRC overlayer*

The transverse strain range evolution at the critical location on UHPFRC top surface (i.e., middle point of path SN) is plotted in Fig. 15, with the mechanical recovery ratio of 70%. Since the strain gauges separated from the UHPFRC top surface after 20,000 cycle, the discussion in this section is focused on the numerical results.

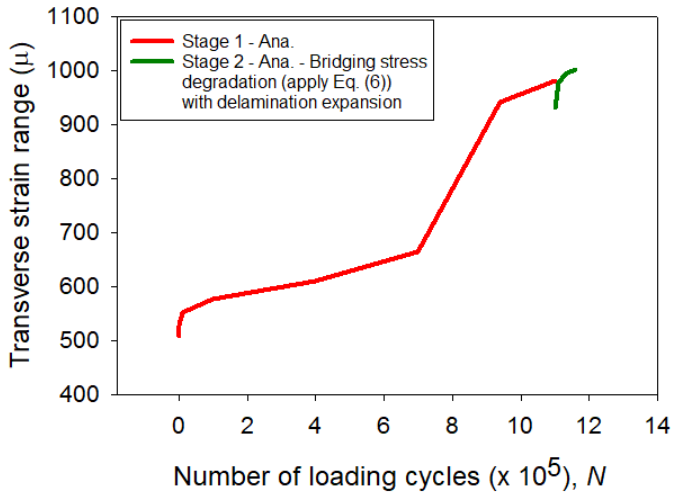


Fig. 15 Transverse strain evolution at the middle point of path SN

In Stage 1, the transverse strain range of the UHPFRC overlayer gradually increase until 700,000th cycle, due to the combination of the degradations of cracked bridging stress and interfacial bond stiffness. After that, from 700,000th to 1,100,000th cycles, a considerable increase in strain range results are obtained after the formation and development of the interfacial delamination area.

In Phase 1 of Stage 2, it can be observed that there is a reduction in transverse strain range at the middle point of path SN in UHPFRC overlayer after applying the mechanical recovery ratios of 70% to the UHPFRC surface cracks to reproduce the self-healing behavior. Herein, the reduction percentage is approximately 5.09% (reduced from 981μ to 932μ). Subsequently, under fatigue loading process (Phase 2), by applying the increased speed of crack bridging stress degradation in Eq. (6), the transverse strain results in UHPFRC overlayer continuously increase, especially from the initial 5,000 cycles of Phase 2. These results are similar to the observation of the steel strain results represented in Fig. 10.

*6.2.3 Numerical and experimental crack region on top surface of UHPFRC*

Fig. 16(a) shows the distributions of the maximum principal strain from the UHPFRC top layer subjected to a moving-wheel load during the beginning and ending cycles of Stage 2. In the analysis, a sequence from load case 10 to load case 12 represents the wheel-load moving process from the east

patch to the center patch (Fig. 7(c)). The gray color indicates the cracked regions on overlayer surface. According to the analysis, the highest level of the maximum principal strain applied to the top layer of the UHPFRC is reported above the middle rib (Rib 4) in load case 12. In load case 13, the maximum principal strain levels and obtained cracking zone are substantially reduced compared to those in the adjacent load cases, owing to the stiffening effect of the middle crossbeam. At the end of Stage 2 with the presence of stagnant water, multiple fine cracks are not localized into macrocracks. Despite the significant increase in the bridging stress degradation speed applied for UHPFRC, the highest level of the maximum principal strain obtained from the reinforced overlayer is still within the strain-hardening domain of the UHPFRC, i.e., lower than 1750μ, at the end of Stage 2; this can be attributed to the high tensile strength, along with high fatigue durability under dry conditions for the UHPFRC. This also agrees with the surface fine cracks (hairline) observed from the experimental crack pattern shown in Fig. 16(b). Herein, it can be seen that the surface cracks occurred at the contact region of rubber tires, while no crack at this region is obtained from the analysis (Fig.16(a)). Moreover, the through-thickness cracks as well as cracks under bottom surface which were obtained in the analysis (Fig. 13) was not observed in the experiment. The possible reason for this issue may be due to the non-uniform distribution of the steel fibers in the UHPFRC overlay. As reported from the bending test of UHPFRC beams (Sakai et al., 2022), the fiber contents near the top surface of the specimens are lower than those from the bottom parts, since the fiber may sink in the matrix due to the high flowability of UHPFRC. Referring to for the current composite deck, the mechanical properties (i.e., elastic modulus, cracking strength, tensile strength…) from the bottom layer of UHPFRC overlayer may be higher than those from the middle and top layers. Hence, further investigations of the composite bridge deck are needed to examine the effect of the non-uniformity of fiber distribution on the cracking behavior of the UHPFRC overlayer.

Generally, in Stage 2, the fatigue deterioration of the tested composite bridge deck is dominated by the bridging stress degradation of fractured UHPFRC on the overlayer surface. Therefore, the

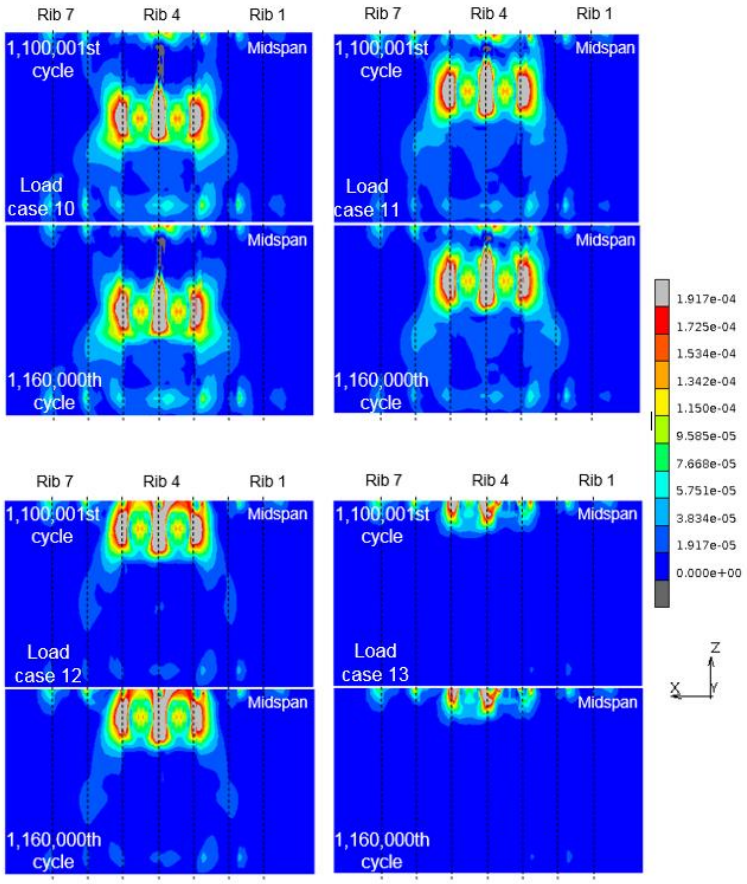


(a) Distributions of maximum principal strain on the UHPFRC top layer obtained from the fatigue analysis (Gray color: the crack region)

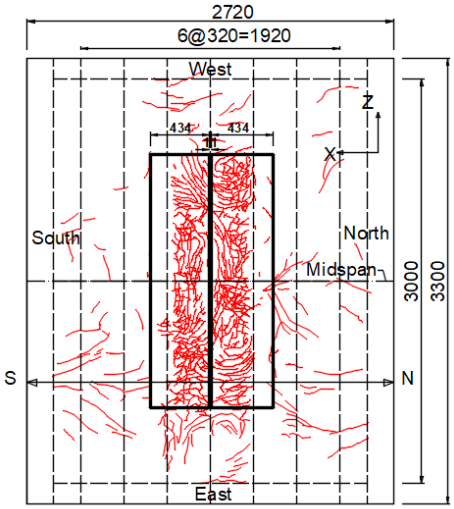


(b) Experimental crack pattern on UHPFRC top surface

Fig. 16 Crack region obtained from: (a) Fatigue analysis; (b) Experiment.

development of the crack region on the top layer of the UHPFRC, which is mainly governed by interfacial degradation, is insignificant throughout this stage owing to the small expansion of the debonded region.

## 7. Conclusions

In this study, a 3D nonlinear FEM analysis was performed to examine the fatigue performance of an OSD reinforced by UHPFRC overlayer under wheel loading and surface water conditions. Two phases of the material model considering the self-healing behavior and reduction in the fatigue life of UHPFRC were introduced in the numerical model. Following this, the considered mechanisms for the material model of cracked UHPFRC were assessed by investigating the UHPFRC cracking behavior and strain range of the steel deck plate based on the fatigue analysis. The following conclusions can be drawn:

(1) The efficient FE calculation which minimize the number of elements as well as the analysis time was proposed, in which the non-uniform distributions along the longitudinal and transverse directions of contact patch of rubber tire was applied for better estimations of critical responses in steel plate and overlayer.

(2) Under surface water condition, the mechanical recoveries of the tensile strength and reloading stiffness caused by the self-healing behavior can result in the reductions in strain ranges of the UHPFRC overlayer and steel plate. It was found in the analysis that the strain range at steel-plate critical location could reduce up to 7.32% with the self-healing recovery ratios of 100% applied for the UHPFRC surface cracks. Correspondingly, the fatigue life of the OSD could be extended to a maximum of 7.87% in surface water condition.

(3) The effect of self-healing on reducing steel strain ranges were more apparent at the three-middle longitudinal ribs where most of UHPFRC surface cracks are located.

(4) Under combined condition of fatigue wheel loading and surface water, the deterioration of the UHPFRC cracks could be accelerated. By considering the reduction rate from the fatigue life of the concrete material under water condition (i.e. about 70%) to that of the UHPFRC, the degradation relation in bridging stress for UHPFRC cracks under the surface water condition was firstly introduced and applied in the current analysis.

(5) In Stage 2, the fatigue deterioration of the tested composite bridge deck is dominated by the bridging stress degradation of fractured UHPFRC on the overlayer surface.

Overall, although there were still discrepancies between the numerical and experimental strain range levels, the proposed mechanisms in the UHPFRC material model could provide a qualitative agreement in terms of strain range tendencies between the analysis and experiment. Therefore, it can be inferred that the proposed behaviors, i.e., self-healing and fatigue life reduction, are reasonable and possible to be considered in the future numerical researches of the OSD reinforced by UHPFRC overlayer under surface water condition.

To improve the numerical modelling of the OSD-UHPFRC composite structure, some recommendations for the future research are as follows:

(1) It is suggested that more fatigue tests of the OSD overlaid by UHPFRC under surface water condition are necessary to be conducted in the future to construct more experimental data for more understanding about the fatigue behavior of the UHPFRC-OSD composite structure under surface water condition, as well as for more reliable validation of the future numerical model.

(2) The static and fatigue shear bond test should be carried out for the epoxy bond technique to investigate the fatigue characteristic of the used epoxy-bond technique, i.e., residual bond slip caused by the bond stiffness degradation.

(3) The effect of the material properties of UHPFRC material, i.e., elastic modulus, tensile strength, non-uniform properties from top and bottom layers, etc., on the cracking behaviors of the UHPFRC overlayer should be further investigated.

(4) The tire contact conditions in the presence of water should be considered in future studies.


## Acknowledgement

The current study in this paper is financially supported by a Research Grant funded by the Kajima Foundation. Besides, the J-THICOM Construction Association also provides the technical assistance for this work. This is gratefully acknowledged by the authors.


## Declaration of conflicting interests

The authors declare that there is no conflict of interest.

## References


Cuenca E and Serna P (2021) Autogenous self-healing capacity of early-age Ultra-High-Performance Fiber-Reinforced Concrete. *Sustainability*, 13, 3061.

Dai J, Saito Y, Ueda T and Sato Y (2005) Static and fatigue bond characteristics of interfaces between CFRP sheets and frost damage experienced concrete. In: *Proceedings of the Fourth International Symposium on Fiber Reinforced Polymer Reinforcement for Reinforced Concrete Structures (FRPRCS-7)*, Missouri, p. 1515-1530.

Deng P and Matsumoto T (2018) Determination of dominant degradation mechanisms of RC bridge deck slabs under cyclic moving loads. *International Journal of Fatigue* 112:328-340.

Deng P, Kaminishi H, Gouda Y and Matsumoto T (2021) Influence of insufficient early-age strength of UHPFRC on rehabilitation of OSDs. In: *Proceedings of the 10$^{th}$ International Conference on Bridge Maintenance, safety and Management*, Sapporo, Japan, 11-18 April.

639 Deng P, Mi H, Mitamura H and Matsumoto T (2022) Stress reduction effects of ultra-high
640 performance fiber reinforced concrete overlaid steel bridge deck developed with a new interfacial
641 bond method. *Construction and Building Materials*, 328, 127104.

642 Dieng L, Marchand P, Gomes F, Tessier C and Toutlemonde F (2013) Use of UHPFRC overlay
643 to reduce stresses in orthotropic steel decks. *Journal of Constructional Steel Research* 89: 30-41.

644 Fairbairn EMR, Toledo Filho RD, Battista RC, Brandao JH, Rosa JI and Formagini S (2006)
645 Experimental and numerical analysis of UHPFRC plates and shells. In: *Symposium of Measuring,*
646 *Monitoring and Modeling Concrete Properties, Proceedings of the 16$^{th}$ European Conference of*
647 *Fracture (ECF16)*, Greece, July 3-7, p. 49-58.

648 Herbert EN and Li VC (2012) Self-healing of Engineered Cementitious Composites in the Natural
649 Environment. In: *G.J. Parra-Montesinos, H.W. Reinhardt, and A.E. Naaman (Eds.): HPFRCC 6,*
650 RILEM p.155-162.

651 Herbert EN and Li VC (2013) Self-healing of microcracks in Engineered Cementitious
652 Composites (ECC) under a natural environment. *Materials* 6: 2831-2845.

653 Japan Society of Civil Engineers (2008) Recommendations for Design and Construction of High
654 Performance Fiber Reinforced Cement Composites with Multiple Fine Cracks (HPFRCC). Publisher:
655 Concrete Committee, Japan Society of Civil Engineers.

656 Japan Society of Steel Construction (1993) Fatigue design guidelines for steel structures.

657 Jimi H, Deng P and Matsumoto T (2021) Bridging stress degradation model of UHPFRC from
658 numerically fitting fatigue flexural test results using FEA. In: *Proceedings of the JSCE Conference*
659 *Hokkaido branch No. 77*, A-46, Japan, January 30 - February 5.

J-THIFCOM Construction Association (2020) The material pamphlet of J-THIFCOM (Japan – Thixotropic Hardening Impermeable Fiber Reinforced Composite). Available at: https://www.j-thifcom.com/tech.html.

Kan LL and Shi HS (2012) Investigation of self-healing behavior of Engineered Cementitious Composites (ECC) materials. *Construction and Building Materials*, 29: 348-356.

Kim S, Yoo DY, Kim MJ and Banthia N (2019) Self-healing capability of ultra-high-performance fiber-reinforced concrete after exposure to cryogenic temperature. *Cement and Concrete Composites*, 104, 103335.

Li M and Li VC (2011) Cracking and healing of Engineered Cementitious Composites under Chloride environment. ACI Materials Journal, 108(3).

Li VC and Matsumoto T (1998) Fatigue crack growth analysis of fiber reinforced concrete with effect of interfacial bond degradation, *Cement and Concrete Composites* 20(5):339-351.

Ma CH, Deng P, Matsumoto T (2021) Fatigue analysis of a UHPFRC-OSD composite structure considering crack bridging and interfacial bond stiffness degradations. *Engineering Structures*, 249, 113330.

Ma CH, Deng P, Ueda K, Mitamura H, Matsumoto T (2021) Finite element analysis on strengthening effect of the UHPFRC-steel composite deck. In: *Proceedings of the 10$^{th}$ International Conference on Bridge Maintenance, safety and Management*, Sapporo, Japan, 11-18 April.

Maekawa K and Fujiyama C (2013) Crack water interaction and fatigue life assessment of RC bridge decks. In: *Proceedings of the Poromechanics V: American Society of Civil Engineers*, Vienna, Austria, 10-12 July.

Makino D, Gouda Y, Mitamura H and Matsui S (2021) Wheel-load-running fatigue test of an UHPFRC-steel composite bridge deck. In: *Proceedings of the 10th International Conference on Bridge Maintenance, safety and Management*, Sapporo, Japan, 11-18 April.

Matsui S (1987) Fatigue strength of RC-slabs of highway bridge by wheel running machine and influence of water on fatigue. In: *Proceedings of Japan Concrete Institute*, 9(2): 627-632, Japan.

Matsui S (1996) Lifetime prediction of bridge. *Journal of Japan Society of Civil Engineers* 30: 432–440.

Matsumoto T and Li VC (1999) Fatigue life analysis of fiber reinforced concrete with a fracture mechanics based model. *Cement and Concrete Composites* 21(4):249-261.

Matsushita H (1980) A study on compressive fatigue strength of concrete in the water. In: *Proceedings of the Japan Society of Civil Engineers*, JSCE, 296: 87-95.

Matsushita H and Tokumitsu Y (1979) A study on compressive fatigue strength of concrete considered survival probability. *Journal of Materials, Concrete Structures and Pavement, Japan Society of Civil Engineers* 284: 127-138.

Mi H (2020) *Finite element analysis on the stress reduction effects of UHPFRC overlaid steel bridge deck developed with a new interfacial bond method*. Master Thesis, Hokkaido University, Hokkaido, Japan.

Mitamura H, Omote S and Nishi H (2011) Effects of Retrofit with Two CFRP Materials of Different Properties on Fatigue Durability Improvement of RC Slabs. In: *Civil Engineering Research Institute (CERI) Monthly Report*, Japan, p. 2-14.

Okuizumi T, Deng P and Matsumoto T (2021) Experimental study about the effects of crack self-healing in UHPFRC on bending behaviors. In: *Proceedings of the JSCE Conference Hokkaido branch No. 77*, A-20, Japan, February.

704 Rots JG and Blaauwendraard J (1989) Crack models for concrete: discrete or smeared? Fixed,
705 multi-directional or rotating? *HERON* 34(1):1-59.

706 Sakai R, Deng P and Matsumoto T (2022) Evaluation of fiber dispersibility of UHPFRC by X-ray
707 CT scan and image analysis. In: *Proceedings of the JSCE Conference Hokkaido branch No. 78*, A-
708 16, Japan, January 29 - 30, 2022.

709 Solwik V and Saouma EV (2000) Water pressure in propagating concrete cracks. *Journal of*
710 *Structural Engineering* 126(2): 235-242.

711 Suthiwarapirak P, Matsumoto T and Kanda T (2004) Multiple cracking and fiber bridging
712 characteristics of Engineered Cementitious Composites under fatigue flexure. *Journal of Materials*
713 *in Civil Engineering*, American Society of Civil Engineers, 16(5).

714 Waagaard K (1982) Fatigue strength evaluation of offshore concrete structures. *American*
715 *Concrete Institute, Symposium Paper* 75: 373-397.

716 Zhang J, Stang H and Li VC (1999) Fatigue life prediction of fiber reinforced concrete under
717 flexural load. *International Journal of Fatigue* 21(10):1033-1049.

718 Zhang J, Stang H and Li VC (2000) Experimental study on crack bridging in FRC under uniaxial
719 fatigue tension. J Mater Civ Eng (ASCE) 2000; 12(1):66-73.

720 Zhang Z and Zhang Q (2017) Self-healing ability of Engineered Cementitious Composites (ECC)
721 under different exposure environments. *Construction and Building Materials*, 156: 142-151.

722